Supplemental Materials

Integrative mouse and computational models link altered myosin kinetics to early events in cardiac disease

Farah Sheikh[1*,§], Kunfu Ouyang[1*], Stuart G. Campbell[2*], Robert C. Lyon[1], Joyce Chuang[1,2], Dan Fitzsimons[3], Jared Tangney[2], Carlos G. Hidalgo[4], Charles S. Chung[4], Hongqiang Cheng[1], Nancy D. Dalton[1], Yusu Gu[1], Hideko Kasahara[5], Majid Ghassemian[6,7], Jeffrey H. Omens[1,2], Kirk L. Peterson[1], Henk L. Granzier[4], Richard L. Moss[3], Andrew D. McCulloch[2§] and Ju Chen[1§]

Departments of [1]Medicine, [2]Bioengineering, [6]Chemistry and [7]Biochemistry, University of California-San Diego, 9500 Gilman Drive, La Jolla, CA, 92093, US; [3]Department of Physiology, University of Wisconsin School of Medicine and Public Health, 1300 University Avenue, Madison, WI, 53706, US; [4]Department of Physiology, University of Arizona, 1656 E. Mabel, Tucson, AZ, 85724; [5]Department of Physiology and Functional Genomics, University of Florida College of Medicine, 1600 SW Archer Road, Gainesville, FL, 32610, US

*These authors contributed equally to this work.

[§]Corresponding authors: Farah Sheikh, Department of Medicine, University of California-San Diego, 9500 Gilman Drive, La Jolla, CA, 92093-0613C, US. Tel: (858) 246-0754, Fax: (858) 822-1355; email address: fasheikh@ucsd.edu; Andrew McCulloch, Department of Bioengineering, University of California-San Diego, 9500 Gilman Drive, La Jolla, CA, 92093-0412, US. Tel: (858) 534-2547; Fax: (858) 332-1706; email address: amcculloch@ucsd.edu and Ju Chen, Department of Medicine, University of California-San Diego, 9500 Gilman Drive, La Jolla, CA, 92093-0613C, US. Tel: (858) 822-4276; Fax: (858) 534-2069; email address: juchen@ucsd.edu.

Supplemental Figure Legends

Supplemental Figure 1. Generation of single (S15A) and double (S14A/S15A) MLC2v phosphorylation mutant knock-in mice. **(A)** MLC2v genomic region of interest (top), the targeting construct (middle), and the mutated S15A locus after homologous recombination (bottom). **(B)** MLC2v genomic region of interest (top), the targeting construct (middle), and the mutated S14A/S15A locus after homologous recombination (bottom). **(C, left)** DNAs isolated from Neo-positive SM ES cell clones were digested with *SstI* and assessed by Southern blotting for wild-type (WT) and heterozygous (HE) alleles with the probe shown in (a). **(C, right)** Tail DNAs isolated from WT and SM mice were also analyzed for WT and SM alleles, respectively, by PCR analyses. **(D, left)** DNAs isolated from Neo-positive DM ES cell clones were digested with *SstI* and assessed by Southern blotting for wild-type (WT) and heterozygous (HE) alleles with the probe shown in (b). **(D, right)** Tail DNAs isolated from WT and DM mice were also analyzed for WT and DM alleles, respectively, by PCR analyses. **(E)** Incorporation of S15A and S14A/S15A knock-in mutations were verified by PCR and sequencing analyses. Mutations are highlighted by asterisks (*).

Supplemental Figure 2. Alignment of mouse striated and smooth muscle/non-muscle myosin light chain phosphorylation sites. Striated myosin light chain isoforms (MLC2v (cardiac) and MLC2F (skeletal)) and smooth muscle/non-muscle myosin light chain isoforms (Myl12B and Myl9) were aligned using Clustal X2 software. After multiple alignments, conserved and aligned residues are depicted in color. A residue is assigned a residue-specific color that is independent of its position (e.g. M,A,V,F,I,L,C,W in blue; K,R in red; S,T,Q,N in green; P in yellow; D,E in magenta; G in orange; Y,H in cyan), and residues are colored based on the alignment consensus at each position.

Supplemental Figure 3. *In vivo* serial echocardiographic assessment of cardiac size and function in SM mutant versus WT mice at two (WT n=9; SM n= 12) and ten (WT n= 9; SM n= 12) months of age. Abbreviations: IVSd: Interventricular septal wall thickness at end-diastole;

LVPWd: Left ventricular (LV) posterior wall thickness at end-diastole; LVIDd: LV internal dimension at end-diastole; LVIDs: LV internal dimension at end-systole; FS (%): LV percent fraction shortening.

Supplemental Figure 4. The DCM phenotype in DM mutant mice is not associated with upregulation of cardiac fetal gene molecular marker expression and fibrosis. **(A)** Atrial natuiretic factor (*ANF*), α-Myosin Heavy Chain (*MHC*), β-*MHC*, cardiac actin (*cActin*), skeletal α-actin (*skActin*) and phospholamban (*PLB*) RNA expression in WT, DM and SM left ventricles (n=3) at three months of age. *Gapdh* RNA was assessed as a loading control. Similar results were obtained in mice at 6 weeks of age (data not shown). **(B)** Masson Trichrome stain of WT, DM and SM mouse heart sections at three months of age. Bar is equivalent to 50μm.

Supplemental Figure 5. A subset of DM mutant mice (DM_S) sporadically display cardiac calcification and fibrosis with a modest re-expression of the fetal cardiac marker, β-MHC. **(A, left)** (left) Gross morphology of WT and DM_s mouse hearts at three months of age. Bar is equivalent to 2mm. **(A, middle left)** Cardiac sections from WT and DM_S mice were stained with the von Kossa stain. Bar is equivalent to 2mm. Red square highlights calcification in ventricular septum endocardium of DM_s mouse heart. **(A, right)** High magnification view of calcification (top, middle) and fibrosis (top, right) in ventricular septum endocardium of DM_s mouse heart (DM_s-Se). Right atrium stained with von Kossa stain (DM_s-RA) displays calcification in this region. Masson Trichrome stain of left atrium (LA) and ventricle (LV) in DM_s mice reveal fibrosis in these regions. Bar is equivalent to 150 μm. **(B)** *skActin*, β-*MHC,* α-*MHC, ANF* RNA expression in representative WT and DM_s left ventricles at 3 months of age. *Gapdh* RNA was assessed as a loading control.

Supplemental Figure 6. Echocardiographic measurements of cardiac dimensions and function in WT (n=14) and DM (n=14) hearts at 6 wks of age. Abbreviations: IVSd: Interventricular septal wall thickness at end-diastole; LVPWd: Left ventricular (LV) posterior wall thickness at end-

diastole; LVIDd: LV internal dimension at end-diastole; LVIDs: LV internal dimension at end-systole; FS (%): LV percent fraction shortening.

Supplemental Figure 7. Twitch dynamics in WT and DM muscles at 37°C. **(A)** Representative isometric twitch tension measured in right ventricular papillary muscles isolated from WT and DM papillary muscles. Traces were recorded following steady-state pacing at 5 Hz. **(B)** Mean characteristics of twitch tension time courses in WT (n=7) and DM (n=6) papillary muscles. DM muscles exhibit significantly reduced time from peak to 50% relaxation and thus accelerated relaxation. Values are represented as mean ± SEM. Abbreviations: TTP-T, time from stimulus to peak tension; TP50-T, time from peak to 50% tension decay. ** $p < 0.001$ vs. WT.

Supplemental Figure 8. Schematic illustrations of the approach and assumptions used to relate MLC2v phosphorylation to power stroke kinetics via phosphorylation-dependent lever arm stiffness. **(A)** A simple energy landscape between pre- and post-power stroke states was assumed for zero stiffness conditions ($\varepsilon = 0$, gray line in top panel). As the myosin lever arm moves between pre- and post-power stroke states (bottom panel), energy is stored in compliant structures within the crossbridge (middle panel) at levels that depend on ε. When ε is nonzero, energy adds to the landscape assumed for conditions of zero stiffness (top panel, red and blue lines) and this causes changes to power stroke kinetic rates. The blue lines in the upper two panels depict the anticipated effects of MLC2v phosphorylation on transition and spring energies as a function of lever arm position. **(B)** Assumptions used in mathematical formulation of stiffness-dependent kinetic rates. Assumptions 1 and 2 are supported by findings in Kaya et al. (57). **(C)** The generic energy landscape with labels showing energy changes used in the model derivation (see text).

Supplemental Figure 9. Uniqueness of fit for optimized MLC2v phosphorylation model parameters. Values of two parameters representing putative molecular effects of MLC2v phosphorylation were adjusted to simultaneously fit responses measured in skinned myocardium treated with myosin light chain kinase (see main text Figure 3, panels D and E).

This plot shows the cumulative error between measured and simulated results as the parameter values for myosin diffusion increase (p_f) and crossbridge stiffness (ε_P) are allowed to vary over a wide range. Error increases monotonically as parameter values are changed in any direction away from the fitted quantities, showing that the fit is robust and unique.

Supplemental Tables

Supplemental Table 1: Myofilament model parameter sets. Parameters were obtained by fitting responses to measurements obtained in skinned mouse myocardial preparations and in right ventricular papillary muscles isolated from DM MLC2v mutant mice. Myosin-related parameters f, h_f, and h_b shown here describe the 'baseline' activity of myosin, i.e. in the absence of MLC2v phosphorylation.

Parameter Name	Values Fitted to Data from Skinned Mouse Myocardium, 15°C	Values Fitted to Data from Intact DM Mouse Papillary Muscle, 25°C	Values Fitted to Data from Intact DM Mouse Papillary Muscle, 37°C	Units
k_{Ca}^{+}	0.09	0.09	0.09	$\mu M\ ms^{-1}$
k_{Ca}^{-}	0.475	0.625	0.625	ms^{-1}
k_{B}^{+}	50	350	750	ms^{-1}
k_{B}^{-}	0.327	0.327	0.327	ms^{-1}
γ_B	50	300	300	-
q	0.5	0.5	0.5	-
f	5.1e-03	1.11e-02	0.1	ms^{-1}
g	1.8e-03	7.8e-03	7.0e-02	ms^{-1}
h_f	5.12e-02	0.22	2.0	ms^{-1}
h_b	1.02e-02	3.33e-02	0.4	ms^{-1}
g_{xb}	5.12e-02	0.122	1.1	ms^{-1}
x_0	8	8	8	nm

Supplemental Table 2: Myosin-related parameters f, h_f, and h_b after applying MLC2v phosphorylation-dependent transformations for each condition according to Eqns. S1 and S2.

Parameter Name	Skinned Mouse Myocardium, 15°C $Q_P = 0.39$	Intact WT Mouse Papillary Muscle, 25°C $Q_P = 0.31$	Intact WT Mouse Papillary Muscle, 37°C $Q_P = 0.31$	Units
f	8.4e-03	1.67e-02	0.165	ms^{-1}
h_f	3.59e-02	0.168	1.42	ms^{-1}
h_b	2.97e-02	7.67e-02	1.13	ms^{-1}

Supplemental Table 3: Parameters and initial conditions for the closed-loop circulatory model (60; with some values modified to agree with mouse hemodynamic parameters).

Parameter description and units	Value
Left Ventricular Pressure (initial) [kPa]	1.34
Volume of aorta (initial) [μl]	35
Volume of vena cava (initial) [μl]	728
Arterial impedance [kPa ms/μl]	2.8
Compliance of aorta [μl/kPa]	3.75
Resistance of aorta [kPa ms/μl]	27.62
Volume of aorta at zero pressure [μl]	0
Compliance of vena cava [μl/kPa]	1744
Resistance of vena cava [kPa ms/μl]	0.5
Volume of vena cava at zero pressure [μl]	0
External pressure [kPa]	0

Supplemental Table 4: Passive material properties of the finite element model of left ventricular mechanics (63).

Parameter and units	Description	Value
C_{pas} [kPa]	Passive stress scaling constant	0.88
$b_{f\,[-]}$	Parameter associated with fiber strain	18.5
b_t [-]	Parameter associated with strain transmural to fiber and shear strain in radial-crossfiber plain	3.58
b_{fr} [-]	Length of series elastic element during isometric contraction	1.63
C_{comp} [kPa]	Bulk modulus	300
$SL_{unloaded}$ [μm]	Unloaded sarcomere length	1.85
α_2		0.2
α_3		0.2
α_s		0.152
α_n		0.152

Supplemental Table 5: Length-dependent contractile model parameters used in the finite element model of the left ventricle (63). Some values were modified to reflect contractile properties of mouse myocardium.

Parameter and units	Description	Value
$a_{Hill\ [-]}$	Parameter that defines the curvature of the Hill relation	1.5
$b_{Hill\ [-]}$	Parameter that determines curvature of the Hill relation during shortening	1.5
L_{s0} [μm]	Contractile element at zero active stress	1.51
$L_{se,iso}$ [μm]	Length of series elastic element during isometric contraction	0.04
v_{max} [μm/sec]	Unloaded sarcomere shortening velocity	75.0
sfact [-]	Force scaling factor	15000

Supplemental Methods

Generation of gene targeted mice. *Mlc-2v* genomic DNA was isolated from a 129-SV/J mouse genomic DNA library, as previously described (51). PCR-based mutagenesis was used to introduce (i) a single mutation (SM) of T to G in codon 15 of *Mlc-2v* as well as (ii) a double mutation (DM) from AG to GC in codon 14 and from T to G in codon 15 of *Mlc-2v* to generate targeted alleles for SM and DM mice, respectively. The SM changed codon 15 from Ser to Ala and simultaneously abolished a *SstI* site, whereas the DM changed codon 14 and 15 from Ser to Ala and also simultaneously abolished a *SstI* site. A pGKneo-tk cassette flanked by two loxP sites was inserted into intron 2 as a selectable marker in both targeted alleles such that it could subsequently be deleted by Cre mediated recombination. The targeting constructs were linearized with *NotI* before electroporation into R1 ES cells. G418-resistant ES clones were screened for homologous recombination by *SstI* digestion, followed by Southern blot analysis as previously described (52). To avoid the interference of the pGKneo-tk cassette with expression of the Ser15 to Ala15 and Ser14/15 to Ala14/15 alleles, the cassette was deleted in ES clones by transient transfection of the cre-encoding plasmid pmc-cre and selection with gancyclovir as described (53). Two independent homologous recombinant ES clones for each line were microinjected into C57BL/6J blastocysts and transferred into pseudopregnant recipients. SM and DM chimeric animals resulting from the microinjection were bred with C57BL/6J mice to generate germ line-transmitted agouti heterozygous SM and DM mice. PCR analysis was performed on tail DNA from mouse offspring from SM and DM intercrosses by using *Mlc-2v* primers (forward, CACTTGGTCATAG TCACTTGTG; reverse, GGATGGATGCTATGCT GCCCAG) using standard procedures. Sequence analysis (Bio Applied Technologies Joint Inc., CA) was performed on PCR products to verify the presence of the mutations in SM and DM mice, using standard procedures. Both SM and DM offspring were backcrossed into the C57BL/6J background. Since SM and DM mice were backcrossed for at least ten generations into the C57BL/6J background, we utilized age-matched wild type C57BL/6J mice (Charles

River Laboratories) as controls for all experiments. All animal procedures were in full compliance with the guidelines approved by UCSD Animal Care and Use Committee.

Two-Dimensional gel analysis. Multicellular myocardial preparations (600–900 mm × 100–250 mm) were isolated and homogenized from mouse hearts as previously described (29). The homogenates were centrifuged at 120 g for 1 min, and the resulting pellet was washed with fresh relaxing solution and resuspended in relaxing solution containing 250 μg saponin/ml and 1% Triton X-100. After 30 min, the skinned preparations were washed with fresh relaxing solution and were dispersed in 50 ml relaxing solution in a glass Petri dish. The dish was kept on ice except during the selection of multiple preparations, which were subsequently placed in rehydration/sample buffer (Bio-Rad Laboratories). Myocardial homogenates were analyzed for non-phosphorylated and phosphorylated MLC-2v states using two-dimensional gel electrophoresis in a mini gel system (Bio-Rad Laboratories) as previously described (Olsson et al., 2004). In brief, the first dimensional iso-electric focusing (IEF) tube gels containing 8 mM urea, 4% acrylamide-bisacrylamide (30% acrylamide/bisacrylamide solution; Bio-Rad Laboratories), 2% Triton X-100, 2% ampholyte (pH 4.1-5.9; Bio-Rad Laboratories), 0.02% ammonium persulfate, and 0.2% TEMED were prefocused first at 200 V for 15 min and then at 400 V for 15 min. The samples were then loaded onto the gels and electrofocused first at 500 V for 20 min and then at 750 V for 4 h 40 min. The IEF tube gels were ejected onto a 12.5% Tris-HCL Criterion Precast gel (Bio-Rad Laboratories) and electrophoresed at 150 V for 1 h 30 min. The gels were then silver stained at room temperature, as described by manufacturer's instructions. The percent MLC-2v phosphorylation was quantified by using densitometry.

Liquid Chromatography (LC)-Tandem Mass Spectrometery (MS/MS) analysis. Myofilament proteins were isolated from mouse hearts as previously described (44). Protein samples were separated by 12 % sodium dodecyl sulfate (SDS)-polyacrylamide gel electrophoresis (PAGE) and visualized by Coomassie blue staining as previously described (44). The gel band corresponding to the MLC-2v protein (19 kDa) was excised and trypsinized as described by Shevchenko *et al.* (45). The extracted peptides were analyzed directly by LC-MS/MS using

electrospray ionization. All nanospray ionization experiments were performed using a QSTAR-Elite™ hybrid mass spectrometer (ABSciex®) interfaced to a nanoscale reversed-phase high-pressure liquid chromatograph (Tempo™) using a 10 cm-180 micron ID glass capillary packed with 5-mm C18 Zorbax™ beads (Agilent®). The buffer compositions were as follows. Buffer A was composed of 98% H_2O, 2% ACN, 0.2% formic acid, and 0.005% TFA; buffer B was composed of 100% ACN, 0.2% formic acid, and 0.005% TFA. Peptides were eluted from the C-18 column into the mass spectrometer using a linear gradient of 5–60% Buffer B over 60 min at 400 ul/min. LC-MS/MS data was acquired in a data-dependent fashion by selecting the 4 most intense peaks with charge state of 2 to 4 that exceeds 20 counts, with exclusion of former target ions set to "360 seconds" and the mass tolerance for exclusion set to 100 ppm. Time-of-flight MS was acquired at *m/z* 400 to 1600 Da for 1s with 12 time bins to sum. MS/MS data were acquired from *m/z* 50 to 2,000 Da by using "enhance all" and 24 time bins to sum, dynamic background subtract, automatic collision energy, and automatic MS/MS accumulation with the fragment intensity multiplier set to 6 and maximum accumulation set to 2 s before returning to the survey scan. Peptide identifications were made using paragon algorithm executed in Protein Pilot 2.0 (Life Technologies) with emphasis on biological modifications and phosphorylation in addition to Mascot™ (Matrix Sciences®). Peptides with confidence levels of above 95% were identified as positive. Raw files and search result files are available as supplementary material if required.

Phosphorylation assays. Myofilament proteins were isolated from mouse hearts as previously described (44). MLC2v kinase reactions were performed at 30°C using 50 μg of myofibrillar protein extract. For assessment of cardiac MLCK phosphorylation, reactions were performed using 1.7 nM of cardiac MLCK in 25 μl of kinase buffer (25mM HEPES, pH7.6, 10 mM $MgCl_2$, 5 mM DTT, 20 mM NaCl, 0.2% triton, 2% glycerol, 0.5 mg/ml BSA and 0.5 mM [γ-^{32}P]-ATP at 267 cpm/pmol). For assessment of skeletal MLCK phosphorylation, reactions were performed using 2 nM of skeletal MLCK in 25 μl of kinase buffer supplemented with 1 mM Ca^{2+} and 1 mM calmodulin. Reactions were terminated after 15 minutes by the addition of SDS-sample buffer.

Samples were separated by 15% SDS-PAGE gel, stained with Coomassie blue, and the level of MLC2v phosphorylation was visualized by autoradiography. The relative amount of phosphorylated and total MLC2v was determined by densitometric analyses. In addition, phosphorylated MLC2v proteins were excised from the gel and their radioactivity measured by liquid scintillation counting.

Electron microscopy. Hearts were first perfused with a high potassium phosphate buffered saline solution containing 77mM NaCl, 4.3mM $Na_2HPO_4 \bullet 7H_2O$, 1.47mM KH_2PO_4 and 62.7 mM KCl, followed by perfusion with 2% paraformaldehyde in 0.1 M sodium cacodylate buffer, pH 7.4. The left ventricle free wall was subsequently cut into 1mm pieces and immersed in a modified Karnovsky's fixative (1.5% glutaraldehyde, 3% paraformaldehyde and 5% sucrose in 0.1 M sodium cacodylate buffer, pH 7.4) for at least 8 hours, postfixed in 1% osmium tetroxide in 0.1 M cacodylate buffer for 1 hour and stained en bloc in 1% uranyl acetate for 1 hour. Hearts were dehydrated in ethanol, embedded in epoxy resin, sectioned at 60 to 70 nm, and picked up on Formvar and carbon-coated copper grids. Grids were stained with uranyl acetate and lead nitrate, viewed using a JEOL 1200EX II (JEOL, Peabody, MA) transmission electron microscope and photographed using a Gatan digital camera (Gatan, Pleasanton, CA).

Measurement of Ca^{2+}-mediated force dynamics in isolated intact papillary muscles. Right ventricular papillary muscles were isolated from mouse hearts, mounted and calibrated in a cardiac tissue culture chamber as previously described (47). After setting the muscle at optimal length, the top and side aspects of the muscle were photographed and digitized to determine muscle cross sectional area. Subsequently pacing was increased to 2 Hz, and the muscle was allowed to equilibrate for an additional 20-30 minutes. Ca^{2+} transients and twitch tension were measured simultaneously in isolated right ventricular papillary muscles at 25°C. For these measurements, the perfusion was stopped and the bathing solution replaced with a loading solution containing the membrane-permeable fluorescent Ca^{2+} indicator Fura-2AM (2 μM final concentration, Invitrogen, Inc.). The muscle was allowed to load at room temperature for 25-30 minutes, after which the bath temperature was set to its corresponding value (25°C) and the

perfusion and pacing were resumed. Muscles were imaged using an extra-long working distance 20X objective. Ratiometric measurement of Fura-2 fluorescence was accomplished by illuminating the muscle with rapidly alternating (333 Hz) 340/380 nm light. Excitation wavelength switching was performed using a fast filter switcher (Lambda DG-4, Sutter Instrument, Inc.). Fura-2 emission (wavelength 540 nm) was then filtered and measured with a photomultiplier tube system (PMT-100, Applied Scientific Instrumentation) and processed by a Data Acquisition Processor (5216a, Microstar Laboratories, Inc.) running custom programs. Experimental protocols, including patterns of pacing and length perturbations, were designed and run using custom software running on the host PC.

Myofilament Ca^{2+} activation computational model with three-state cross bridge cycle. A recently published two-state actin-myosin crossbridge cycling computational model of myofilament Ca^{2+} activation (21) was expanded to include a 3-state crossbridge model (54) to gain insight into the molecular actions of MLC2v phosphorylation. This modification consisted of a detached crossbridge state and two attached states, pre-power stroke and post-power stroke (*C*, M_{pr}, and M_{po} respectively, Figure 3C). A limitation of the three state model is that it does not represent phosphate and ADP release steps separately, but it has the advantage of using a relatively small number of free parameters. For our purposes it was sufficient to consider release of both metabolites as occurring in the same step as the power stroke, an approach that has been used by several others (e.g. Rice *et al.*, 54). Simulated relative contractile force was computed as the fraction of crossbridges in the post-power stroke state. The original features of the computational model showed that Ca^{2+} activation events were more potent than crossbridge binding events in producing cooperative activation of the nearest-neighbor interactions between overlapping tropomyosin molecules along the actin filament as well as other physiological behavior. The new version of the model makes the simplification that only Ca^{2+} activation events are communicated among nearest neighbors, a property described by the coefficient γ_B (Supplemental Table 1). The behavior of several interacting myosin binding sites is represented using a Markov model (21). Whereas each binding site was previously assumed to reside in one

of three states (blocked, closed, or open), the above simplification allows closed and open states to be merged and the number of total Markov model states is reduced substantially. All simulations reported here were performed assuming 13 interacting myosin binding sites with periodic boundary conditions (55). Merging closed and open states necessitated definition of a new conditional probability, μ, which describes the fraction of binding sites in this state that are capable of transitioning to a blocked state. The quantity μ is analogous to the conditional probability ϕ given previously (21) and is defined by:

$$\mu = \frac{P\{C\}}{P\{CM\}}$$

where $P\{C\}$ is the probability associated with the *C* state and $P\{CM\}$ is the global probability associated with the lumped closed/open state as described by the Markov model states. Model parameters and their values are listed in Supplemental Table 1. Rates of Ca^{2+} binding and dissociation from troponin C (k_{Ca}^{+} and k_{Ca}^{-}), as well as rates governing tropomyosin shifting between blocked and closed positions (k_B^{+} and k_B^{-}) were based on values determined previously[21], with only minor modifications to account for species-specific differences. The three-state crossbridge model (54) introduced five new model parameters, including f (crossbridge attachment rate), g (detachment rate of pre-power stroke crossbridges), h_f (forward power stroke rate), h_b (reverse power stroke rate), and g_{xb} (detachment of post-power stroke crossbridges). Parameter values were coarsely adjusted to produce a crossbridge duty cycle (average fraction of cycle time spent bound to actin) of ~20%, in accordance with previous modeling work (21). All simulations assumed constant sarcomere length, meaning that force is produced in proportion to the occupancy of the M_{po} state. Force produced by the model was calculated as the product of average individual crossbridge stiffness (ε , Equation S2), the number of crossbridges per unit cross-sectional area (N_{xb}), crossbridge distortion induced by

the power stroke (x_0), and the fraction of total crossbridges in the attached, post-powerstroke state ($P\{M_{po}\}$):

$$F = N_{xb}\varepsilon x_0 P\{M_{po}\}$$

The value of N_{xb} was set to 6.25×10^{16} in order to match mean peak twitch tension at 4 Hz pacing frequency and 25°C bath temperature.

Three model parameters (f , h_f , and h_b) were identified as potentially dependent on MLC2v phosphorylation. Crossbridge attachment rate (f) was assumed to increase with MLC2v phosphorylation due to increased diffusion of the myosin head away from the thick filament backbone (Mechanism 1, Figure 3A), according to the equation

$$f = f_{base}\left(1 + p_f Q_P\right) \qquad \text{(Eqn. S1)}$$

where f_{base} is the baseline (non-phosphorylated) value (Supplemental Table 1), p_f is a weighting coefficient scaling the effect of phosphorylation, and Q_P is the fractional MLC2v phosphorylation level.

We used the hypothesis of phosphorylation-dependent lever arm stiffness (56) as a basis for altering power stroke rates h_f and h_b in a phosphorylation-dependent manner (Mechanism 2, Figure 3B). The recent work of Kaya *et al.* (57) on the stiffness of individual myosins provided a biophysical framework for mathematically relating Q_P to power stroke kinetic rates. They found that while imposing loads on actin-myosin crossbridges reduced the *observed* power stroke distance, this could be explained by deformation in a compliant region in myosin S1 while the underlying conformational changes during power stroke produced a load-independent *working* stroke distance of 8 nm. Accordingly, we assumed that phosphorylation of MLC2v increases the stiffness of the myosin lever arm (56) without changing the working stroke distance.

(*Observed* or 'unitary' step size increase, as discussed by Greenberg *et al.* (56) and others, would still be expected to occur). Under these assumptions, phosphorylation of MLC2v alters the energy landscape between pre- and post-power stroke states in a straightforward manner that allows determination of kinetic rates (Figure S7). Values for the forward and reverse power stroke kinetic rates (h_f and h_b, respectively) under conditions of zero MLC2v phosphorylation were determined previously by fitting model responses to published data from skinned myocardium (see above). The energy landscape reflected by these kinetic coefficients (see Figure S7) is assumed to include the energetic cost of straining the myosin crossbridge with stiffness ε_{BS} (2 pN nm^{-1}) by the working stroke, x_0 (8 nm, (57)). At this baseline stiffness (BS), the energy difference between pre- (pr) and post- (po) powerstroke states is given by the Gibbs relation as:

$$\Delta G_{pr/po}\Big|^{BS} = -\ln\left(K_{pr/po}^{BS}\right)RT$$

where $K_{pr/po}^{BS}$ is the equilibrium constant h_f / h_b and R and T are the gas constant and temperature, respectively. The increase in free energy associated with straining the crossbridge during powerstroke can be determined assuming linear elasticity as

$$\Delta G_{spr} = \frac{1}{2}\varepsilon_{BS} x_0^2 .$$

The free energy change under conditions of zero crossbridge stiffness (ZS) can subsequently be determined by subtracting the contribution of the strained crossbridge,

$$\Delta G_{pr/po}\Big|^{ZS} = \Delta G_{pr/po}\Big|^{ZS} - \Delta G_{spr}$$

Next, an estimation of the activation energy required to undergo powerstroke under baseline stiffness conditions can be performed using the Eyring equation solved for the activation energy as follows:

$$\Delta G_f^{\dagger}\Big|^{BS} = -\ln\left(\frac{h_f h}{k_B T}\right) RT$$

We make the assumption that the conformational energy barrier coincides with straining the crossbridge half the distance of the working stroke, $1/2 x_0$. Hence the contribution of crossbridge strain to the activation energy is given by

$$\Delta G_{act,spr} = \frac{1}{2}\varepsilon_{BS}\left(\frac{1}{2}x_0\right)^2 = \frac{1}{8}\varepsilon_{BS}x_0^2 = \frac{1}{4}\Delta G_{spr}$$

Then, the ZS forward activation energy is found by subtracting $\frac{1}{4}\Delta G_{spr}$ from the BS activation energy:

$$\Delta G_f^{\dagger}\Big|^{ZS} = \Delta G_f^{\dagger}\Big|^{BS} - \frac{1}{4}\Delta G_{spr}$$

Now that ZS conditions have been determined, it is possible to express the relative activation and state energies as functions of crossbridge stiffness ε . The activation energy for forward power stroke as a function of the crossbridge stiffness is

$$\Delta G_f^{\dagger}(\varepsilon) = \Delta G_f^{\dagger}\Big|^{ZS} + \frac{1}{4}\Delta G_{spr}$$

once again assuming that the conformational energy barrier coincides with half of the working stroke distance. The ZS activation energy for the reverse power-stroke transition is simply the ZS forward activation energy minus the ZS free energy change:

$$\Delta G_b^{\dagger}\Big|^{ZS} = \Delta G_f^{\dagger}\Big|^{ZS} - \Delta G_{pr/po}^{ZS}$$

Increasing stiffness increases the transition threshold by $\frac{1}{4}\Delta G_{spr}$ and the energy of the post power-stroke state by ΔG_{spr}, so the reverse activation energy as a function of stiffness is

$$\Delta G_b^{\dagger}(\varepsilon) = \Delta G_b^{\dagger}\Big|^{ZS} + \Delta G_{spr} - \frac{1}{4}\Delta G_{spr}, \text{ or}$$

$$\Delta G_b^{\dagger}(\varepsilon) = \Delta G_b^{\dagger}\Big|^{ZS} + \frac{3}{4}\Delta G_{spr}.$$

Once the activation energies are known, stiffness-dependent rates can be obtained by using the Eyring equation again:

$$h_f(\varepsilon) = \frac{k_B T}{h}\exp\left(\frac{-\Delta G_f^{\dagger}(\varepsilon)}{RT}\right)$$

$$h_b(\varepsilon) = \frac{k_B T}{h}\exp\left(\frac{-\Delta G_b^{\dagger}(\varepsilon)}{RT}\right)$$

The average crossbridge stiffness ε is determined by the stiffness under phosphorylated and non-phosphorylated conditions weighted by the proportion of phosphorylated MLC2v:

$$\varepsilon = \varepsilon_{BS}\left(1 - Q_p\right) + \varepsilon_P\left(Q_p\right) \qquad \text{(Eqn. S2)}$$

Values for p_f and ε_P were determined by comparing simulation output with experimental measurements in skinned mouse myocardium at 15°C reported by Stelzer *et al* (29). Parameters of the myofilament model were first adjusted to fit the force-Ca^{2+} relation observed in the absence of MLC2v phosphorylation (Supplemental Table 1, main text Figure 3E, red line). Leaving all other model parameters unchanged, Q_P was set to 0.39 and p_f (Mechanism 1)

and ε_P (Mechanism 2) were adjusted until responses observed at 39% MLC2v phosphorylation were matched to >2.5% cumulative error (main text, Figure 3D). Fit error was calculated as the absolute difference between simulated and measured quantities, normalized by the measured quantity and expressed as a percentage. Cumulative error was the sum of fit errors for the quantities of maximum tension, maximum k_{tr} (rate of force redevelopment), and myofilament Ca^{2+} sensitivity. Final fitted values were $p_f = 1.632$ (unitless) and $\varepsilon_P = 2.462$ pN nm^{-1}, and were used to represent phosphorylation in all remaining simulations. The result of applying equations S1 and S2 to model parameters can be seen in final form in Supplemental Table 2.

In order to evaluate the importance of cooperative interactions among neighboring tropomyosins in mediating the phosphorylation response, we performed an additional simulation in which cooperativity was removed by setting $\gamma_B = 0$ (see main text, Figure 3D).

To ensure that fitted values of p_f and ε_P were unique, and not reflective of a local minimum in the error landscape, we computed the cumulative error for more than 3,600 pairs of wide-ranging p_f and ε_P values (Figure S8). Deviations from fitted values of either parameter caused the cumulative error to increase sharply and monotonically, demonstrating the uniqueness of fitted parameters.

Muscle twitch dynamic simulations using new computational model. Baseline parameters of the new model (Figure 3C) were first coarsely adjusted to reflect increased steady-state Ca^{2+} sensitivity and cooperativity observed in intact cardiac muscle (58), and twitch forces were simulated by driving the model with a representative Ca^{2+} transient recorded in WT preparation paced at 4 Hz and 25°C. Parameters were then fine-tuned such that a simulated twitch matched a representative record from a DM papillary muscle at the same temperature and pacing rate (Supplemental Table 1). A WT twitch was then predicted simply by increasing Q_P from 0 to 0.31 (the value measured in WT mouse myocardium), which altered crossbridge kinetics according to the sensitivities determined earlier (above).

Urea Glycerol Gel Analysis Method to Quantify MLC2v Phosphorylation. Urea glycerol gel methods were done essentially as previously described (30,49). Briefly, mouse hearts (3 months old) were rapidly excised, arrested [35 mM KCl, 100 mM NaCl, 0.36 mM NaH_2PO_4, 1.75 mM $CaCl_2$, 1.08 mM $MgCl_2$, 21 mM $NaHCO_3$, 5 mM glucose, 5U/L insulin and 0.08g/L BSA] and mounted on a Langendorff perfusion system utilizing 90mmHg constant pressure perfusion at 37ºC. A small custom plastic balloon was inserted into the left ventricle (LV) chamber through the mitral orifice. Hearts were perfused with an oxygenated Tyrode solution (7.4 mM KCl, 127 mM NaCl, 0.36 mM NaH_2PO_4, 1.75 mM $CaCl_2$, 1.08 mM $MgCl_2$, 21 mM $NaHCO_3$, 5 mM glucose, 5U/L insulin and 0.08g/L BSA) and paced at 250 bpm. Hearts were allowed to equilibrate and stabilize with 5-10mmHg preload. A Frank-Starling protocol was utilized to determine the appropriate volume for 0mmHg preload. Upon cessation of contractions, pacing was turned off and volume was changed to the appropriate preload in hearts for 30 minutes and then immediately flash frozen in liquid N_2. Endocardial and epicardial segment sections were performed on frozen hearts in 60% glycerinating solution in relaxing solution including 84 mM leupeptin, 20 mM, E-64 and 80 mM PMSF. Approximately 20 mg of frozen tissue was pulverized to a fine powder and solubilized in 50% glycerol containing 84 mM leupeptin, 20 mM E-64, and 80 mM PMSF and 620 ml of freshly prepared urea sample buffer (9 M urea, 50 mM Tris pH 8.6, 300 mM glycine, 5 mM DTT, and 0.001% bromophenol blue). The proteins were separated by urea glycerol PAGE. Myosin regulatory light chain 2 ventricular (MLC2v) and the MLC2v phosphorylated (MLC2vP) bands were identified by western blot and Pro-Q Diamond stain. Specific mouse MLC2v monoclonal antibodies (1:1000) that recognizes human and rat ventricular MLC2v (amino acids 45-59) (Enzo Life Sciences, Ab manufactured by BioCytex) were used for western blot analysis. To determine the relative phosphorylation level of MLC2v in epi- and endocardial tissues, the gels were stained with Coomassie blue according to manufacturer's instructions. The densitometry analysis of the protein bands was carried out with 1Dscan EX (Scanalytics Inc., Rockville, MD, USA) software. A range of loadings was used per sample and the integrated OD for each loading was determined. The linear range of the OD-loading relation was determined and the slope (m) of this relation was calculated by using linear

regression analysis. The slope of the MLC2v and the MLC2vP was used to obtain the percentage of MLC2vP according to:

MLC2vP (%) = (mMLC2vP x 100)/(mMLC2vP + mMLC2v).

Computational model of LV torsion. A finite element model of the mouse left ventricle (LV) was generated. LV geometry was approximated as a thick-walled, truncated ellipse of revolution whose dimensions (wall thickness, focal length, and end-diastolic volume) were based on MR-derived anatomical data obtained as a part of this study. A transmural pattern of myofiber orientation was assumed based on published gradients in the murine LV free wall (59). A closed loop, lumped parameter model of the circulation was used to provide appropriate ventricular afterload (60). Mouse-specific parameter values for the circulatory model were derived from published in vivo measurements (61) and are listed in Supplemental Table 3. A five millisecond-delay in activation was assumed across the thickness of the LV wall, based on typical conduction velocities in mouse myocardium (62). Ca^{2+} and length-dependent myocardial contractile force throughout the ventricular mesh was simulated using the same new model of myofilament Ca^{2+} activation, with baseline parameters adjusted to reproduce twitch dynamics measured at 37°C (Supplemental Table 1 and Supplemental Figure 6). Passive material properties of the myocardium were based on previous work (63; see Supplemental Table 4). Equations from the simple Hill-type model of Lumens et al. (64) and modified by Kerckhoffs et al. (63) were added to the myofilament model to represent length- and velocity-dependent behavior of active contraction. This was done by adopting the following equations:

$$L_{se}^{norm} = \frac{L_s - L_{sc}}{L_{se,iso}}$$

where L_{se}^{norm} is the relative length of an elastic element in series with the contractile element, $L_{se,iso}$ is the length of the series elastic element under isometric conditions, and L_s is the sarcomere length as determined from myocardial strain in the finite element model. A differential equation defines the rate of change in the series elastic element as follows:

$$\frac{dL_{sc}}{dt} = \begin{cases} \dfrac{v_{\max}\left(L_{se}^{norm}-1\right)}{b_{Hill}L_{se}^{norm}+1}\exp\left[a_{Hill}\left(L_{se}^{norm}-1\right)\right] & if\ L_{se}^{norm} \geq 0 \\ \dfrac{v_{\max}\left(L_{se}^{norm}-1\right)}{b_{Hill}L_{se}^{norm}+1} & if\ L_{se}^{norm} < 0 \end{cases}$$

Here, b_{Hill} and a_{Hill} are shaping parameters that give the proper curvature to the force-velocity relation. Parameter values are given in Supplemental Table 5. The equation for total active tension, $\sigma_{f,act}$ was modified from the original by substituting their contractility variable *C* for the fraction of post-power stroke crossbridges, M_{pr}, while also scaling by the average crossbridge stiffness ε:

$$\sigma_{f,act} = \sigma_{act} \cdot \varepsilon \cdot M_{po} \cdot \left(L_{sc} - L_{sc0}\right) \cdot \frac{L_s - L_{sc}}{L_{sc,iso}}$$

where L_{sc0} is the slack sarcomere length and σ_{act} is a scaling factor used to scale active tension to achieve an appropriate level of contractility.

A single cardiac beat was simulated by applying a realistic Ca^{2+} transient (58), regionally adjusted for activation delay, to each point throughout the mesh. The time course of myocardial deformation was obtained through solution of model equations under this time-varying input. Ventricular torsion was calculated using the same method as described for the MR tagging measurements. Two separate simulations were performed. In the first, MLC2v phosphorylation was assumed to vary linearly across the thickness of the LV wall, with 30% phosphorylation at the endocardium and 45% at the epicardium. This transmural difference of 15% phosphorylated MLC2v is based on measurements made in isolated rat (30) and mouse ventricle (Figure 4A). In the second simulation, phosphorylation was assumed to be zero at all locations in the ventricle to mimic conditions in the mutant mouse. The density of myofiber stroke work density (SWD) was calculated for each point in the finite element mesh as the area under the curve formed by

plotting contractile tension ($\sigma(t)$) as a function of Lagrangian fiber strain ($\varepsilon(t)$) during the cardiac cycle:

$$SWD = \int \sigma(t) d\varepsilon(t)$$

Magnetic Resonance (MR) Imaging and left ventricle (LV) torsion analysis. *In vivo* murine cardiac imaging was performed on a 7T horizontal-bore MR scanner (Varian magnet with a Buker console), equipped with a 21 cm bore. Mice were anesthetized with isoflurane and imaged in a 2.5 cm Bruker volume coil. Body temperature and the electrocardiogram were monitored. Heart rate was maintained around 400bpm. Cine anatomical imaging was performed using the Fast Low Angle Shot sequence (FLASH) with flip angle = 15°, echo time = 2.8 ms, repetition time = 6 ms, data matrix = 128 x 128, field of view = 2.0 cm, slice thickness = 1 mm, and 4 averages. Myocardial tagging was performed using spatial modulation of magnetization (SPAMM) (65). The tag thickness was 0.3 mm and tag line separation was 0.7 mm, which allowed for 2-3 taglines to be placed across the ventricular wall of the mouse heart. Parameters for the image acquisition were the same as the cine acquisition except for the inclusion of the tagging module and the number of averages was increased to 20. During imaging, the long axis of the left ventricle was first identified. Both cine and SPAMM tagged short axis images were then taken at the base and apex of the left ventricle. Six-week old wild type and mutant mice were scanned (n=6 for each group). For one mouse, the total imaging time was approximately 30 minutes. Tag intersections near the epicardium of the LV free wall are tracked from end diastole to end systole in the basal and apical slice. Torsion was calculated as the circumferential angular displacement between two points, one near the base and one near the apex, normalized by the vertical distance separating them (66). LV volumes were estimated from long axis MR images using Simpson's disc summation method:

$$V = \sum_{i=1}^{n} \frac{\pi t}{4} D_i^2$$

This method approximates the LV cavity by a stack of *n* discs, each having their own diameter D_i. The thickness of each disk, *t*, is the distance corresponding to a single image pixel. Disc diameters are taken as the horizontal distance between endocardial boundary points along a single line of pixels in the long axis MR image. Estimated end-diastolic volumes (EDV) and end-systolic volumes (ESV) were then used to calculate % ejection fraction (EF) according to the formula:

$$EF = \frac{EDV - ESV}{EDV} \times 100\%$$

Supplemental References

51. Chen J, et al. Selective requirement of myosin light chain 2v in embryonic heart function. *J Biol Chem.* 1998;273(2):1252-1256.

52. Zhou Q. et al. Ablation of Cypher, a PDZ-LIM domain Z-line protein, causes a severe form of congenital myopathy**.** *J Cell Biol.* 2001;155(4):605-612.

53. Chen J, Kubalak SW, Chien KR. Ventricular muscle-restricted targeting of the RXRalpha gene reveals a non-cell-autonomous requirement in cardiac chamber morphogenesis. *Development* 1998;125(10):1943-1949.

54. Rice JJ, Wang F, Bers DM, de Tombe PP. Approximate model of cooperative activation and crossbridge cycling in cardiac muscle using ordinary differential equations. *Biophys J.* 2008;95(5):2368-2390.

55. Vibert P, Craig R, Lehman W. Steric-model for activation of muscle thin filaments. *J Mol Biol.* 1997;266(1):8-14.

56. Greenberg MJ, Mealy TR, Jones M, Szczesna-Cordary D, Moore JR. The direct molecular effects of fatigue and myosin regulatory light chain phosphorylation on the actomyosin contractile apparatus. *Am J Physiol Regul Integer Comp Physiol.* 2010;298(4):R989–R996.

57. Kaya M, Higuchi H. Nonlinear elasticity and an 8-nm working stroke of single myosin molecules in myofilaments. *Science.* 2010;329(5992):686-689.

58. Gao WD, Perez NG, Marban E. Calcium cycling and contractile activation in intact mouse cardiac muscle. *J Physiol (Lond).* 1998;507(Pt 1):175-184.

59. Strijkers GJ, et al. Diffusion tensor imaging of left ventricular remodeling in response to myocardial infarction in the mouse. *NMR Biomed.* 2009;22(2):182-190.

60. Kerckhoffs RC, Neal ML, Gu Q, Bassingthwaighte JB, Omens JH, McCulloch AD. Coupling of a 3D finite element model of cardiac ventricular mechanics to lumped systems models of the systemic and pulmonic circulation. *Ann Biomed Eng.* 2007;35(1):1-18.

61. Segers P, et al. Conductance catheter-based assessment of arterial input impedance, arterial function, and ventricular-vascular interaction in mice. *Am J Physiol Heart Circ Physiol.* 2005;288(3):H1157-H1164.

62. Morley GE, Vaidya D, Samie FH, Lo C, Delmar M, Jalife J. Characterization of conduction in the ventricles of normal and heterozygous Cx43 knockout mice using optical mapping. *J Cardiovasc Electrophysiol* 1999;10(10):1361-1375.
63. Kerckhoffs RC, Omens JH, McCulloch AD, Mulligan LJ. Ventricular dilation and electrical dyssynchrony synergistically increase regional mechanical nonuniformity but not mechanical dyssynchrony: a computational model. *Circ Heart Fail.* 2010;3(4),528-536.
64. Lumens J, Delhaas T, Kirn B, Arts T. Three-wall segment (TriSeg) model describing mechanics and hemodynamics of ventricular interaction. *Ann Biomed Eng.* 2009;37(11):2234-2255.
65. Axel L, Dougherty L. MR imaging of motion with spatial modulation of magnetization. *Radiology.* 1989;171(3):841-845.
66. Zhong J, Liu W, Yu X. Characterization of three-dimensional myocardial deformation in the mouse heart: an MR tagging study. *J Magn Reson Imaging.* 2008;27(6):1263-1270.

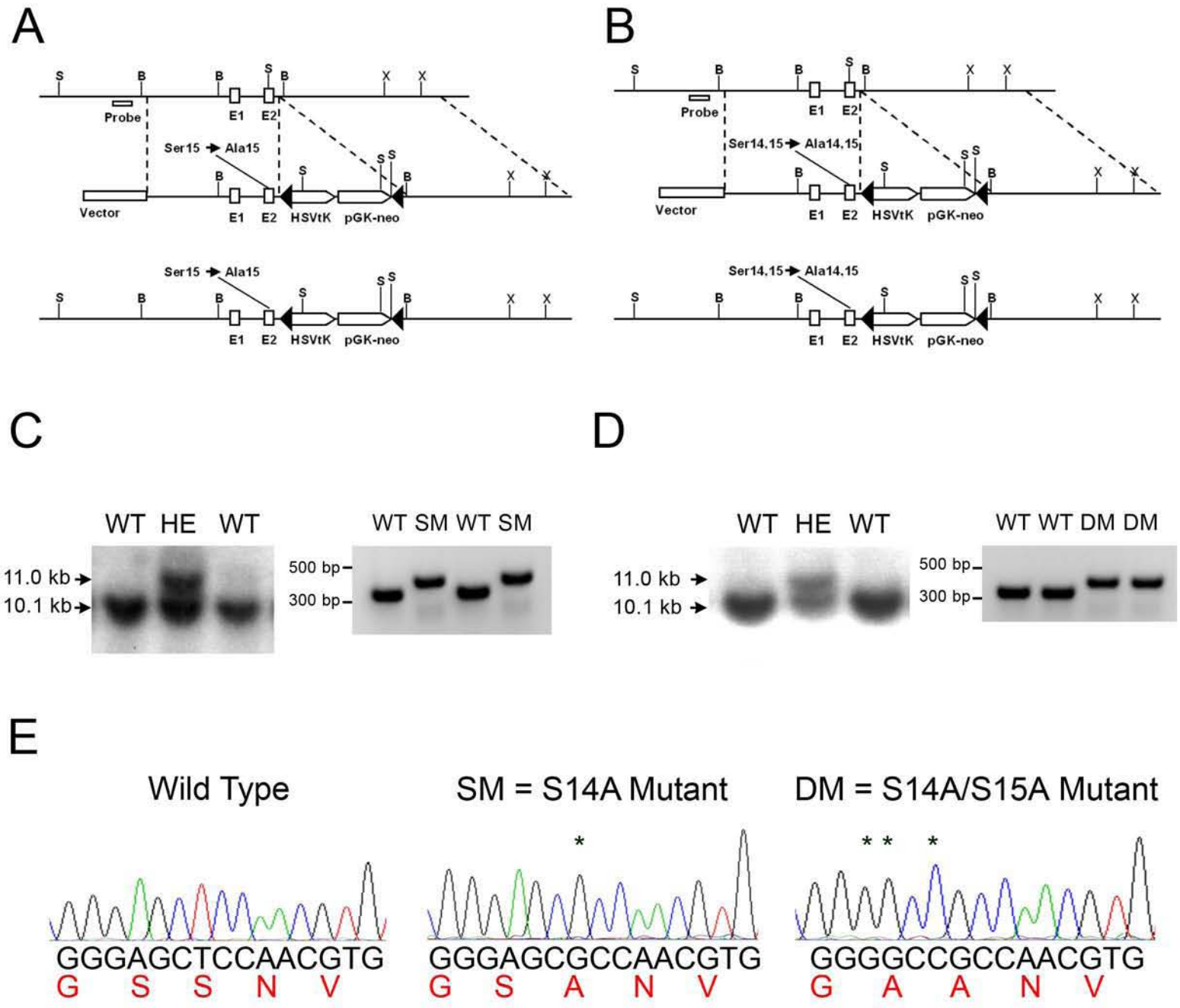

Supplemental Figure 1. Generation of single (S15A) and double (S14A/S15A) MLC2v phosphorylation mutant knock-in mice. **(A)** MLC2v genomic region of interest (top), the targeting construct (middle), and the mutated S15A locus after homologous recombination (bottom). **(B)** MLC2v genomic region of interest (top), the targeting construct (middle), and the mutated S14A/S15A locus after homologous recombination (bottom). **(C, left)** DNAs isolated from Neo-positive SM ES cell clones were digested with SstI and assessed by Southern blotting for wild-type (WT) and heterozygous (HE) alleles with the probe shown in (a). **(C, right)** Tail DNAs isolated from WT and SM mice were also analyzed for WT and SM alleles, respectively, by PCR analyses. **(D, left)** DNAs isolated from Neo-positive DM ES cell clones were digested with SstI and assessed by Southern blotting for wild-type (WT) and heterozygous (HE) alleles with the probe shown in (b). **(D, right)** Tail DNAs isolated from WT and DM mice were also analyzed for WT and DM alleles, respectively, by PCR analyses. **(E)** Incorporation of S15A and S14A/S15A knock-in mutations were verified by PCR and sequencing analyses. Mutations are highlighted by asterisks (*).

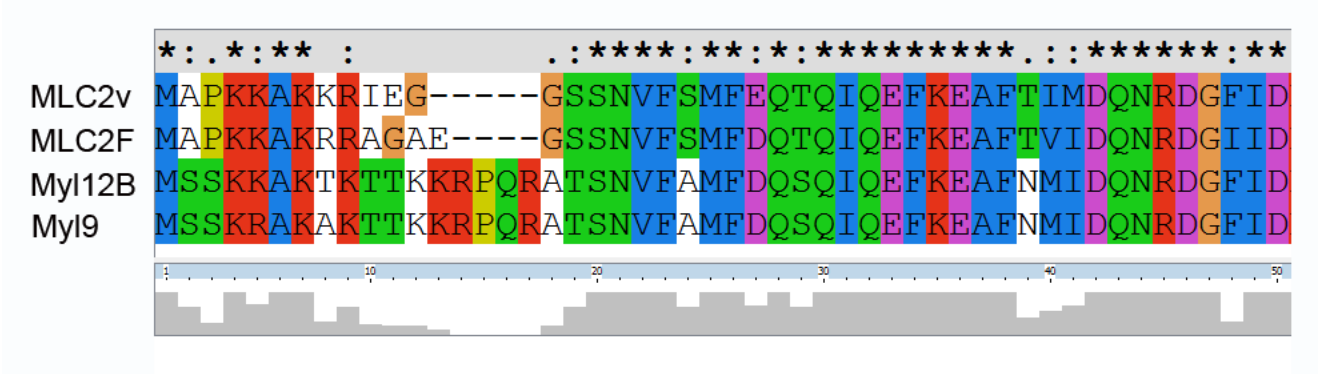

Supplemental Figure 2. Alignment of mouse striated and smooth muscle/non-muscle myosin light chain phosphorylation sites. Striated myosin light chain isoforms (MLC2v (cardiac) and MLC2F (skeletal)) and smooth muscle/non-muscle myosin light chain isoforms (Myl12B and Myl9) were aligned using Clustal X2 software. After multiple alignments, conserved and aligned residues are depicted in color. A residue is assigned a residue-specific color that is independent of its position (e.g. M,A,V,F,I,L,C,W in blue; K,R in red; S,T,Q,N in green; P in yellow; D,E in magenta; G in orange; Y,H in cyan), and residues are colored based on the alignment consensus at each position.

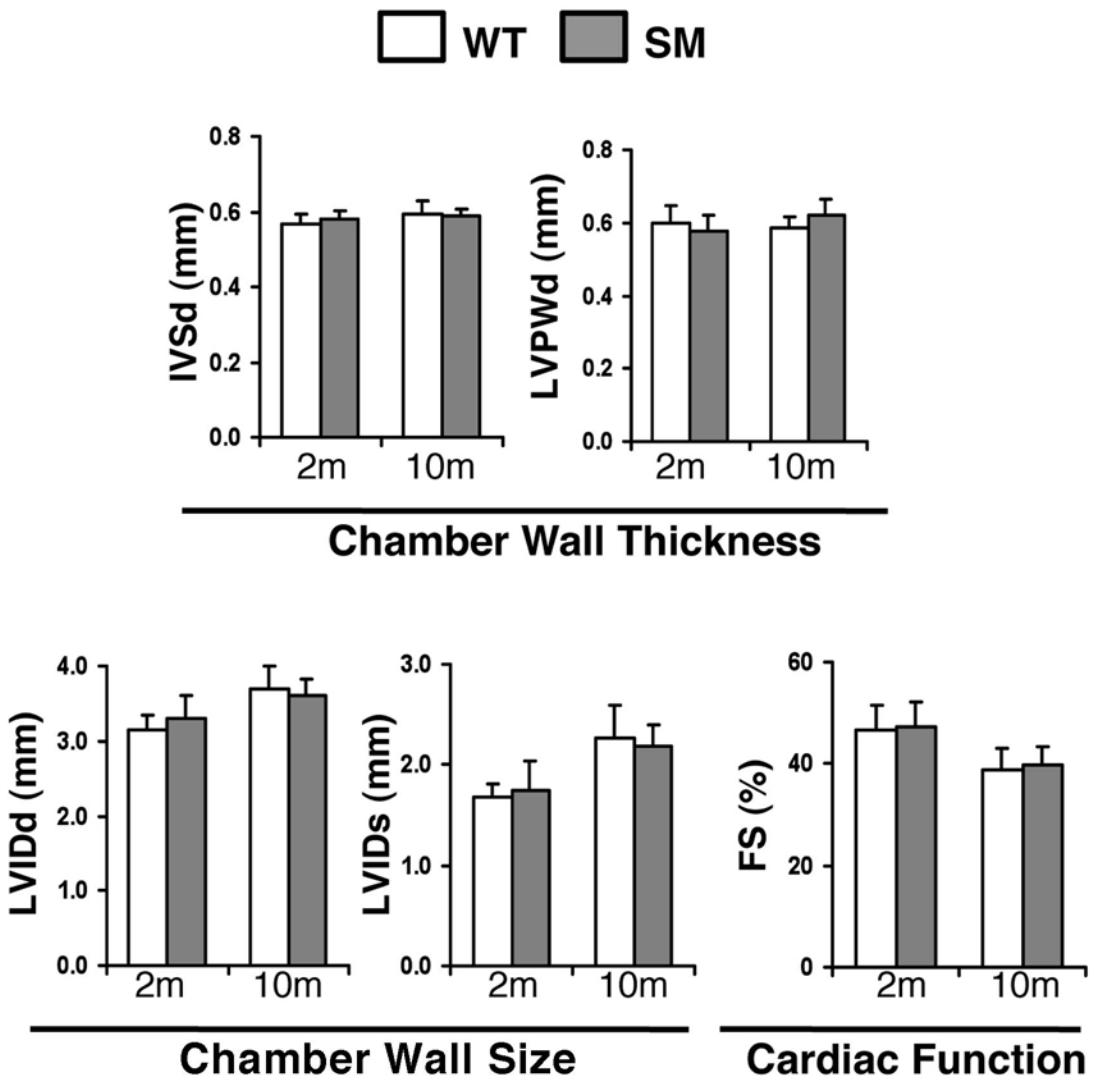

Supplemental Figure 3. In vivo serial echocardiographic assessment of cardiac size and function in SM mutant versus WT mice at two (WT n=9; SM n= 12) and ten (WT n= 9; SM n= 12) months of age. Abbreviations: IVSd: Interventricular septal wall thickness at end-diastole; LVPWd: Left ventricular (LV) posterior wall thickness at end-diastole; LVIDd: LV internal dimension at end-diastole; LVIDs: LV internal dimension at end-systole; FS (%): LV percent fraction shortening.

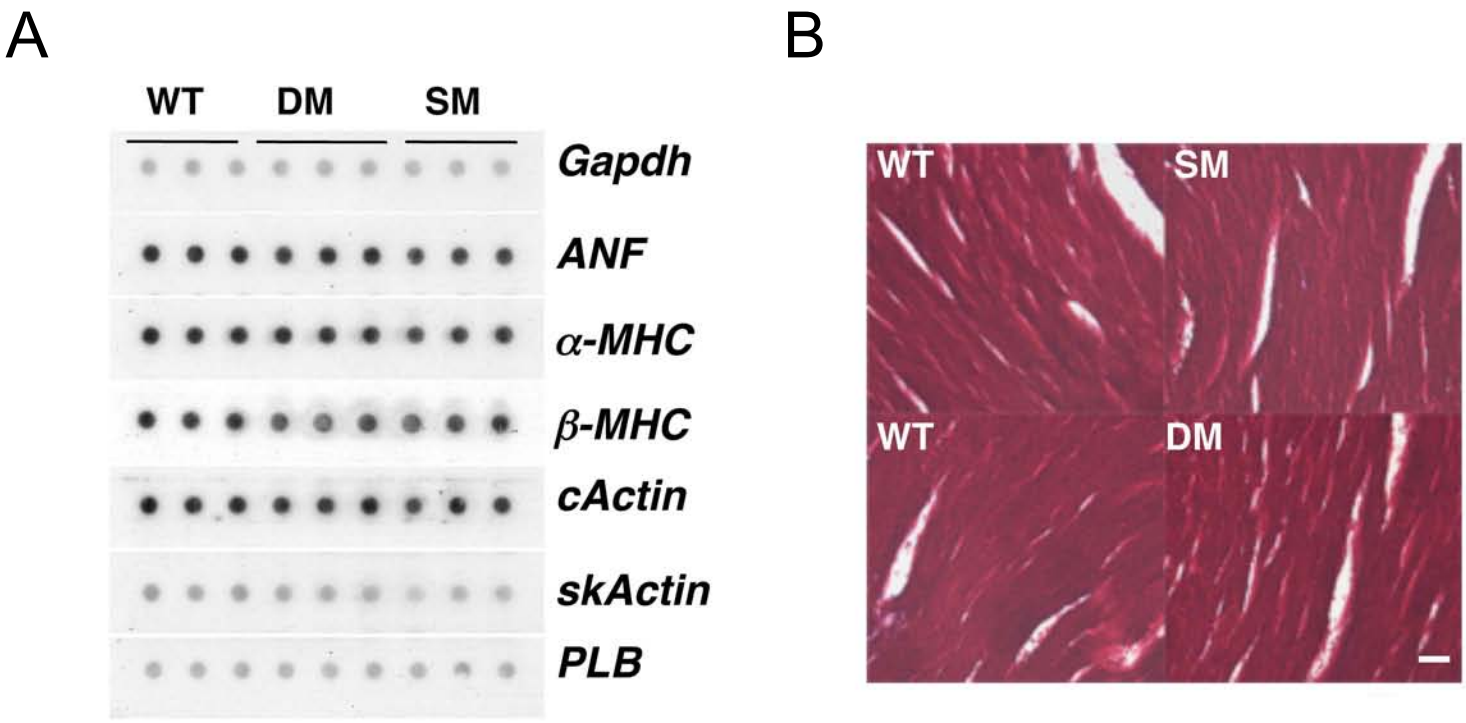

Supplemental Figure 4. The DCM phenotype in DM mutant mice is not associated with upregulation of cardiac fetal gene molecular marker expression and fibrosis. **(A)** Atrial natuiretic factor (ANF), α-Myosin Heavy Chain (MHC), β-MHC, cardiac actin (cActin), skeletal α-actin (skActin) and phospholamban (PLB) RNA expression in WT, DM and SM left ventricles (n=3) at three months of age. Gapdh RNA was assessed as a loading control. Similar results were obtained in mice at 6 weeks of age (data not shown). **(B)** Masson Trichrome stain of WT, DM and SM mouse heart sections at three months of age. Bar is equivalent to 50μm.

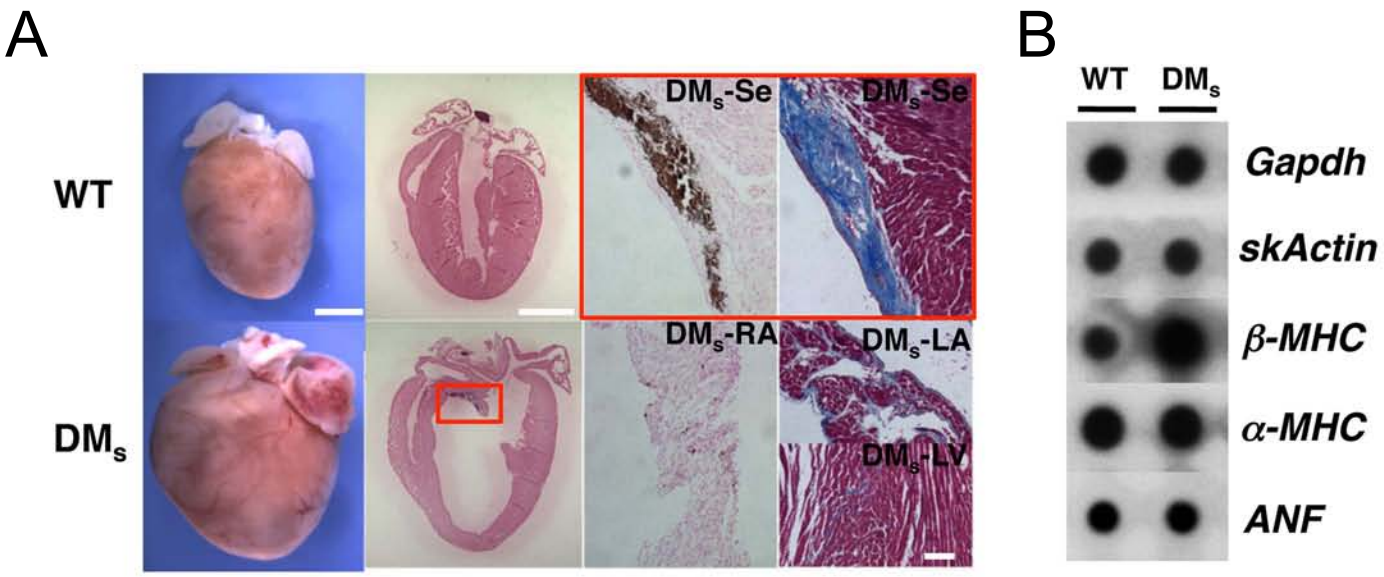

Supplemental Figure 5. A subset of DM mutant mice (DM_S) sporadically display cardiac calcification and fibrosis with a modest re-expression of the fetal cardiac marker, β-MHC. **(A, far left)** Gross morphology of WT and DMs mouse hearts at three months of age. Bar is equivalent to 2mm. **(A, middle left)** Cardiac sections from WT and DMS mice were stained with the von Kossa stain. Bar is equivalent to 2mm. Red square highlights calcification in ventricular septum endocardium of DMs mouse heart. **(A, right)** High magnification view of calcification (top, middle) and fibrosis (top, right) in ventricular septum endocardium of DMs mouse heart (DMs-Se). Right atrium stained with von Kossa stain (DMs-RA) displays calcification in this region. Masson Trichrome stain of left atrium (LA) and ventricle (LV) in DMs mice reveal fibrosis in these regions. Bar is equivalent to 150 µm. **(B)** skActin, β-MHC, α-MHC, ANF RNA expression in representative WT and DMs left ventricles at 3 months of age. Gapdh RNA was assessed as a loading control.

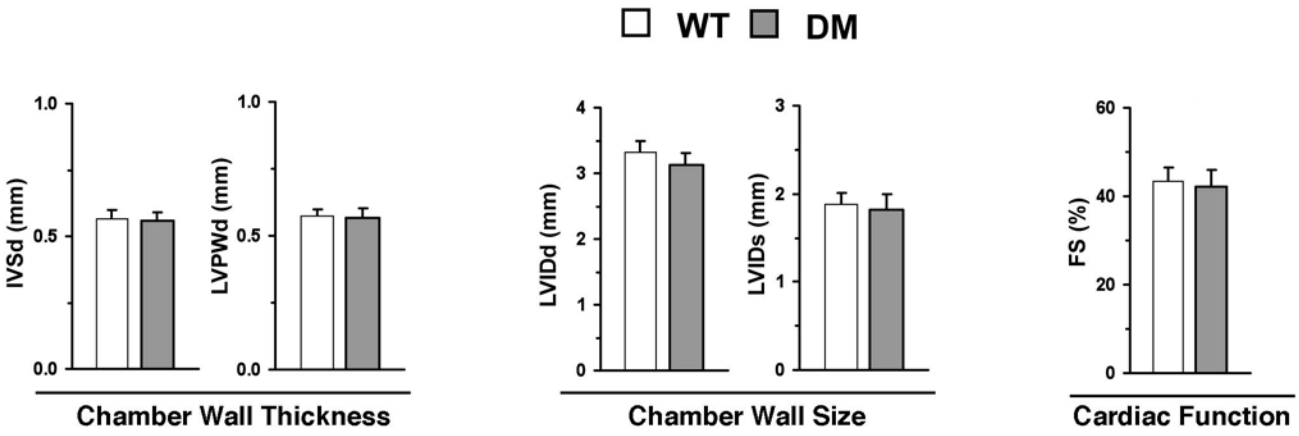

Supplemental Figure 6. Echocardiographic measurements of cardiac dimensions and function in WT (n=14) and DM (n=14) hearts at 6 wks of age. Abbreviations: IVSd: Interventricular septal wall thickness at end-diastole; LVPWd: Left ventricular (LV) posterior wall thickness at end-diastole; LVIDd: LV internal dimension at end-diastole; LVIDs: LV internal dimension at end-systole; FS (%): LV percent fraction shortening.

A

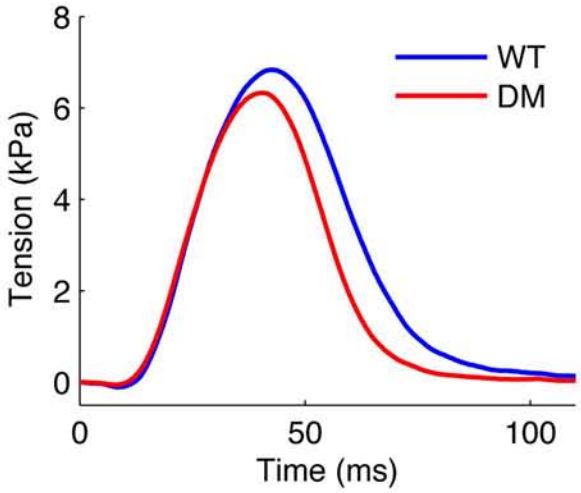

B

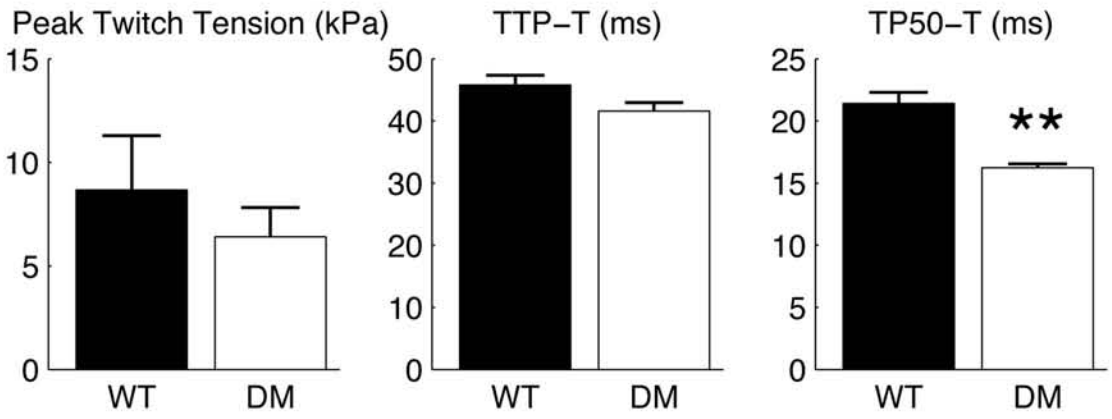

Supplemental Figure 7. Twitch dynamics in WT and DM muscles at 37°C. **(A)** Representative isometric twitch tension measured in right ventricular papillary muscles isolated from WT and DM papillary muscles. Traces were recorded following steady-state pacing at 5 Hz. **(B)** Mean characteristics of twitch tension time courses in WT (n=7) and DM (n=6) papillary muscles. DM muscles exhibit significantly reduced time from peak to 50% relaxation and thus accelerated relaxation. Values are represented as mean ± SEM. Abbreviations: TTP-T, time from stimulus to peak tension; TP50-T, time from peak to 50% tension decay. ** $p < 0.001$ vs. WT.

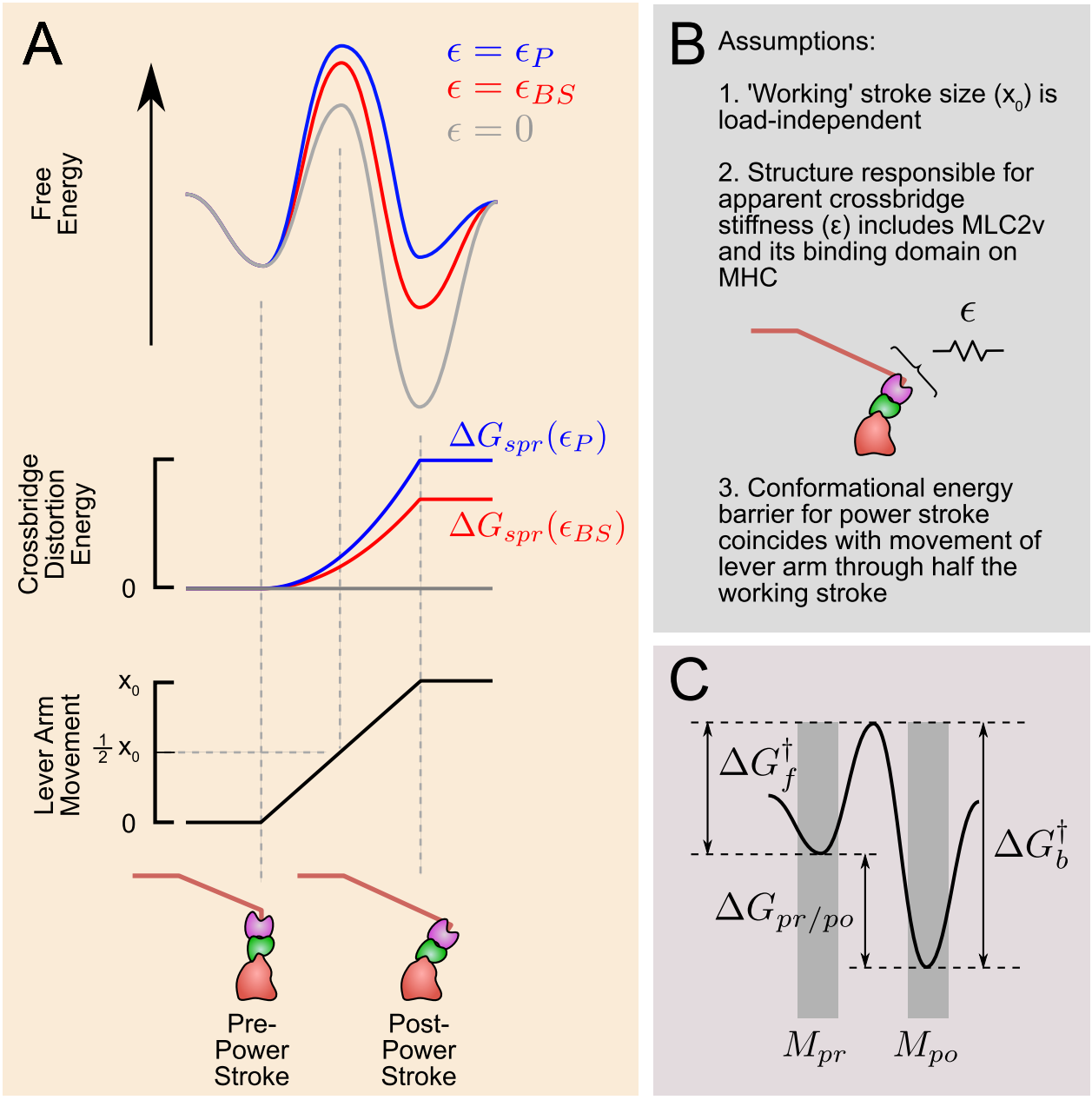

Supplemental Figure 8. Schematic illustrations of the approach and assumptions used to relate MLC2v phosphorylation to power stroke kinetics via phosphorylation-dependent lever arm stiffness. **(A)** A simple energy landscape between pre- and post-power stroke states was assumed for zero stiffness conditions (ε = 0, gray line in top panel). As the myosin lever arm moves between pre- and post-power stroke states (bottom panel), energy is stored in compliant structures within the crossbridge (middle panel) at levels that depend on ε. When ε is non-zero, energy adds to the landscape assumed for conditions of zero stiffness (top panel, red and blue lines) and this causes changes to power stroke kinetic rates. The blue lines in the upper two panels depict the anticipated effects of MLC2v phosphorylation on transition and spring energies as a function of lever arm position. **(B)** Assumptions used in mathematical formulation of stiffness-dependent kinetic rates. Assumptions 1 and 2 are supported by findings in Kaya et al. (57). **(C)** The generic energy landscape with labels showing energy changes used in the model derivation (see text).

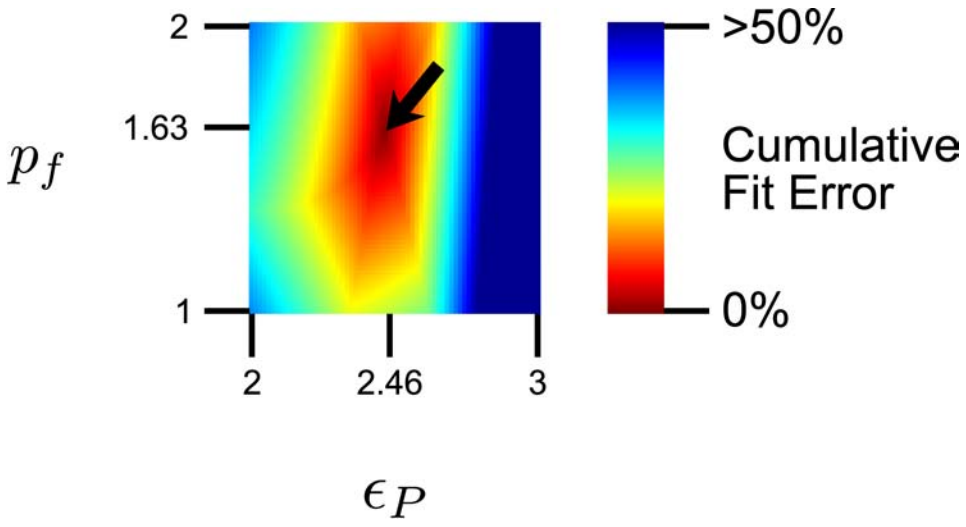

Supplemental Figure 9. Uniqueness of fit for optimized MLC2v phosphorylation model parameters. Values of two parameters representing putative molecular effects of MLC2v phosphorylation were adjusted to simultaneously fit responses measured in skinned myocardium treated with myosin light chain kinase (see main text Figure 3, panels D and E). This plot shows the cumulative error between measured and simulated results as the parameter values for myosin diffusion increase (p_f) and crossbridge stiffness (ε_p) are allowed to vary over a wide range. Error increases monotonically as parameter values are changed in any direction away from the fitted quantities, showing that the fit is robust and unique.